Atmospheric dynamics leading to West European summer hot temperatures since 1851

M Carmen Alvarez-Castro, Davide Faranda, Pascal Yiou

Atmospheric dynamics leading to West European summer hot temperatures since 1851

M. Carmen Alvarez-Castro, Davide Faranda, Pascal Yiou

Laboratoire des Sciences du Climat et de l'Environnement, UMR 8212

CEA-CNRS-UVSQ, IPSL, Université Paris-Saclay, F-91191 Gif-sur-Yvette, France

E-mail: carmen.alvarez-castro@lsce.ipsl.fr

November 2017

Abstract. Summer hot temperatures have many impacts on health, economy (agriculture, energy, transports) and ecosystems. In western Europe, the recent summers of 2003 and 2015 were exceptionally warm. Many studies have shown that the genesis of the major heat events of the last decades was linked to anticyclonic atmospheric circulation and to spring precipitation deficit in southern Europe. Such results were obtained for the second part of the 20th century and projections into the 21st century. In this paper, we challenge this vision by investigating the earlier part of the 20th century from an ensemble of 20CR reanalyses. We propose an innovative description of Western-European heat events applying the dynamical system theory. We argue that the atmospheric circulation patterns leading to the most intense heat events have changed during the last century. We also show that the increasing temperature trend during major heatwaves is encountered during episodes of Scandinavian blocking, while other circulation patterns do not yield temperature

trends during extremes.

Keywords: Weather Regimes, Climate Dynamics, Heat Events

1. Introduction:

In western Europe, recent hot summers were characterized by anomalous meteorological conditions. In those situations, such as 2003, the heat was prolonged and intense, and the consequences were disastrous for society and ecosystems (Schär & Jendritzky 2004, Ciais et al. 2005, Poumadere et al. 2005, Robine et al. 2008, Wreford & Adger 2010).

European surface temperature variations are influenced by processes that combine radiative forcing, the large-scale atmospheric circulation and local phenomena. Over the last five decades, most of the intense European heat events have been connected to prolonged spells of anticyclonic circulation (Scandinavian blocking) and dry spring conditions in Southern Europe (Schär et al. 1999, Fischer et al. 2007, Vautard et al. 2007, Zampieri et al. 2009, Mueller & Seneviratne 2012, Quesada et al. 2012). However, the Summer 2011 was cool and preceded by a dry spring; the Summer 2013 was warm and preceded by a wet spring; and the Summer 2015 was warm with persisting southerly atmospheric flows and no lasting blocking episodes (Jézéquel et al. 2017). The goal of this paper is to assess the robustness of the link between heat events and atmospheric circulation. We perform a statistical and dynamical analysis on a long period that covers 1851–2014. Since anticyclones extend to a radius of few hundreds kilometers, such a connection must be investigated on a regional scale (Della-Marta

et al. 2007, Stefanon et al. 2012). Hence, we restrict our analysis to Western Europe in the region covering France and the Iberian Peninsula, whose weather conditions are strongly influenced by the atmospheric circulation over the North Atlantic. This analysis also puts some of the results of Horton et al. (2015) on this link into a broader time perspective.

2. Data and Methods:

We base our analysis on the sea-level pressure (SLP) and the surface temperature fields during summers (June-July-August: JJA) in 20th Century Reanalysis data version 2c (20CRv2c: 1851–2014, (Compo et al. 2011)) with 2° of resolution and bias correction applied in the sea ice distribution by assimilating new SST and sea-ice cover (SIC) data (Hirahara et al. 2014). To ensure the robustness of the results, we used the ensemble mean (EM) and the 56 members of the ensemble. The analysis is completed with other reanalysis products: NCEP (1948–2016) (Kalnay et al. 1996) and ERA20C reanalysis (1900–2000) (Poli et al. 2013) (see supplementary material). In order to describe the variability of the atmospheric circulation, we decompose the summer SLP anomalies field (obtained by removing the seasonal cycle) into four weather regimes following the approach of Yiou et al. (2008) and study their connection with heat events at seasonal(i) and sub-seasonal(ii) timescales in Western-Europe [10°W – 7.5°E; 35 – 50°N]. i) Seasonal: the 24 summers with high mean temperature anomalies (with respect to the climatology) of the period 1851–2014, and ii) Subseasonal: heatwaves defined as

periods with high temperatures anomalies for at least five consecutive days. In both analyses temperatures are detrended by removing a linear trend calculated from the time series of summer seasonal means. The goal of the detrending is to remove the effect of the well-documented European temperature increase, which does not depend on the weather pattern.

2.1. Weather Regimes:

Weather regimes are recurring states of the atmospheric circulation and provide a useful description of the atmospheric variability (Michelangeli et al. 1995, Corti et al. 1999). Following the methods of Michelangeli et al. (1995) and Yiou et al. (2008) we compute four weather regimes ($k = 4$) over the North Atlantic region [80°W – 50°E; 20 – 70°N] (Fig. 1a-d) on daily NCEP SLP anomalies (reference period: 1970–2010) over the summers (June–July–August: JJA). We take the first ten Empirical Orthogonal Functions (EOFs) of SLP anomalies (with weights that are proportional to the cosine of latitude) and the corresponding Principal Components (PCs). Then we perform a classification, with a k-means algorithm (Michelangeli et al. 1995), and a choice of four weather regimes. This classification is iterated several times with random initial conditions following the procedure of Yiou et al. (2008) in order to obtain weather regimes that are stable. The choice of four weather regimes is to be consistent with the seminal paper of (Cassou et al. 2005). For comparison, we classify different reanalysis datasets with the NCEP weather regimes. All the reanalysis data are interpolated

onto the NCEP grid ($2.5° \times 2.5°$). The SLP data classifications of all reanalyses are obtained by determining the minimum of the Euclidean distances to the four NCEP summer weather regime centroids. This is achieved without further EOF truncation. The NCEP summer weather regimes are shown in Fig. 1a-d, with the same nomenclature as in Cassou et al. (2005): a) the negative phase of North Atlantic Oscillation (NAO−) showing a dipole between Greenland and Northern Europe, b) the Atlantic Ridge (AR), with a high pressure over the center of the North Atlantic and some common features with the positive phase of NAO, c) Scandinavian Blocking (BLO), with a high pressure center over Scandinavia, d) Atlantic Low (AL), with a low pressure center covering the central North Atlantic.

To ensure that there are no inhomogeneities in the method, we have verified that the root mean square error (RMSE) between the reference period and the other periods/datasets is small (Fig. S1 and Table S1).

2.2. Projection onto weather regimes for a dynamical representation:

In order to visualize the dependence between the daily SLP fields and the four weather regimes, we represent the *trajectory* of each summer in the space of correlations (Fig. 3a-h) using an approach based on dynamical systems theory (Katok & Hasselblatt 1997) . In this framework, the motion of a particle is represented in the space defined by its position and speed (the so-called phase space). In our set-up, the particle is replaced

by a SLP field and the directions in phase space correspond to the projections on the four weather regimes. Trajectories provide additional information with respect to the monthly average statistical quantities, on the time dependence and the coherence of the dynamical projection with respect to weather regime bases. If a trajectory jumps every day to a different region of the phase space, then a dominant weather regime is not representative of the dynamical behavior of events lasting several days. If instead the trajectory occupies a restricted region of the phase space with smooth transitions of the projection among weather regimes, then the dynamical representation is informative and the base of weather regimes is appropriate.

This is equivalent to assuming the existence of a low-dimensional attractor. The caveat is that the weather regime description is a first order simplification of the atmospheric circulation that captures large scale features. Although this phase-space method has been debated since Lorenz (1991), there is theoretical (Chekroun et al. 2011) and experimental (Casdagli et al. 1991) evidence that such a procedure is effective when the dynamics can be projected on a low dimensional phase space with a stochastic perturbation.

3. Results and Discussion:

The link between the North Atlantic atmospheric circulation and heat events over France and the Iberian Peninsula is investigated at short and long timescales. Both timescales carry a physical and societal relevance.

3.1. Seasonal scale: weather regimes during the warmest summers

We carried out a statistical analysis of the hottest summers of the period 1851–2014 using 56 members and the Ensemble Mean (EM) of the 20CRv2c. In Western-Europe [10°W – 7.5°E; 35 – 50°N], the 24 warmest summers (Fig. 1e-f) are defined in each dataset as the ones having the highest average temperature anomalies with respect to the climatology. Figure 1e shows the probability to have a dominant weather regime, which is the one with highest anomalous frequency, in each summer detected. From the selection of the 24 warmest summers for each member we detect 52 different summers. In order to show the agreement between the members, we calcule the probability to have a summer dominated by each weather regime (Fig. 1e). We divide the number of members that detects a weather regime dominating that summer by the total number of members that has detected that summer as a warm summer. For instance, we find that for 30 members, the summer of 1887 is one of the 24 warmest summers. For 21 of those 30 members NAO− is the dominant weather regime and BLO for the other 9 members. However, we find a total agreement within 51 members detecting 2003 as a warmer summer with AL as the unique weather regime dominating the summer. Hence, as figure 1e shows, there is a higher probability to find a total agreement within the members after 1950, being mainly BLO the dominant regime of warmest summers during the second half of the 20^{th} century and also briefly during the end of the 19^{th} century. NAO− and AR are the most dominant regimes during the first half of the 20^{th} century. This is also evident when we study the EM (Fig. 1f-j). Figure 1f shows the dominant

weather regime (colors) for the warmest summers (circle size) of the EM(20CRv2c, see Figure S2i of supplementary material for NCEP, ERA20C and 20CR and Figure S3 for some examples of warmest summers). We have divided the warmest summers detected (vertical bars and figure 1g-j) in 4 groups, in order to study the variability during short periods of 30 years. Boxplots in Figures 1g-j indicate the daily frequency of weather regimes by group. In groups G1 (fig. 1g), G3 (fig.1j) and G4 (fig. 1j) BLO is the most frequent regime during warmest summers, while in group G2 NAO− and AR are the most representatives ones. Most of the warmest summers (largest circles in Fig. 1f) occur during the second part of the 20th century. As observed by Stott et al. (2004) and Meehl & Tebaldi (2004), they also increase in frequency over time.

Figure 2a-e) (Figure S2a-d for NCEP and figure S2e-h for ERA20C) shows the anomalous summer frequency of weather regimes in EM of 20CRv2c with respect to the NCEP reference period. In this figure we see that NAO− is the unique regime decreasing in frequency with the time, and BLO is the one increasing in frequency with the time (see also Figures S4 and S5).

To understand such trends we decompose the average information found with the statistical analysis via the dynamical representation of the warmest summers (Fig 3 and Fig. S6), defined in section 2.2. We project the daily SLP anomaly fields (grey lines) onto the 4 weather regimes (NAO− and AR regimes in Fig. 3a,c,e,g and BLO and AL regimes in Fig. 3b,d,f,h). This analysis synthesizes the trajectory of the atmospheric circulation during heat events (colors) in a space represented by the weather regimes.

Circles in the axes represents the average correlations of warmest summers.

Consistently with the previous analysis, we find that the atmospheric dynamics has evolved from patterns that are positively correlated with NAO− during the late 19th century and the beginning of the 20th century(Groups G1 and G2, Fig. 3 a,c), to negative correlations during the rest of the record (Fig. 3 e,g). Similar projections on BLO and AL regimes show: that BLO has the opposite change of NAO− (mainly in groups G2 and G3), being negative during the early period of 20^{th} century (Fig. 3d) and positive during the middle and late 20^{th} century (Fig. 3f-h). AR and AL regimes do not show significant differences between the periods. Those correlations add a daily temporal information and highlight a change of atmospheric behavior. Thus the dominant weather regime is a valid concept as the trajectories of heatwaves persist at sub-seasonal scales around the same region of the phase space. These changes are consistent within the 20CRv2c ensemble, as the analysis of the 56 members (Fig. 4a) shows consistent results with the EM. In Figure 4 we represent the average correlations of warmest summers as for figure 3 (circles in the axes) but for all the 56 members and the EM. As for the EM, the 56 members have a positive o negative correlation to NAO− and BLO depending of the period (groups in colors) being clearly separated in the cloud of points the first to groups (G1 and G2, hereinafter P1) to the two last groups (G3 and G4, hereinafter P2) that happens around 1930. Therefore, if we study now the daily frequency of weather regimes classifying the warmest summers by only two periods; before (P1) and after (P2) 1930, we find similar results as in figure 3 and

4a, opposite frequencies between NAO− and BLO. Higher frequencies of NAO− are detected in P1 for 56 members (Fig. 4c) and the EM (Fig. 4e), and higher frequencies of BLO are detected in P2 for 56 members (Fig. 4d) and the EM (Fig. 4f).

To complement this weather regimes analysis, we compute the difference of the mean SLP for EM between these two periods during the warmest summers, $\Delta_{SLP} = \mu_{SLP(P2)} - \mu_{SLP(P1)}$. We obtain a BLO regime pattern (Fig. 4g) using the EM or 56 members (not shown here). This means that it is the most representative pattern for the period P2, being the period P1 similar to the NAO−.

Therefore, our analysis shows significant changes in the dominating weather regimes associated with warmest summers. If BLO is dominant from the second part of 20th century, scarce occurrences of this weather regime are found before 1930, with the exception of a small period at late 19th century, even within the ensemble members of 20CRv2c. These results reflect a change in the regime frequencies and dominance conducing to warm extremes in a multidecadal scale due to, most likely, an internal variability. BLO and AL regimes are conducive to warm extremes and NAO− and AR are the opposite (Cassou et al. 2005). We found that, after 1930, it is more frequent to find hottest summers linked to what we know as warm regimes. BLO (the most frequent one after 1930) leads to stagnant air and potential land-surface feedbacks, whereas AL relies on advection from lower latitudes. In the other hand, NAO− is the dominant weather regime during warmest summers up to 1930. This weather regime contributes to a weakening of the westerly flow from the Atlantic into Western Europe. AR regime

is more stable in time.

3.2. Subseasonal scale: weather regimes during heatwave events

To understand whether those results hold also for short time events (at least 5 consecutive days), independently from the fact that they have been observed during hot summers, we compute the average temperature during heatwaves striking Western-Europe.

Heatwave events are defined when the summer temperature exceeds a threshold based on percentiles (P90, P95) for more than 5 consecutive days. Figure 5 shows heatwave events above the P95 threshold, computed on the area temperature anomalies (mean of France and the Iberian Peninsula) for the 56 members (Fig 5a-d) and for the EM (Fig. 5e) (See Figure S7 of supplementary material). Temperatures in figure 5 are average values during each heatwave event. Heatwaves events are grouped by the dominating weather regime. We find that 11% of total events are dominated by NAO− (Fig. 5a), 49%, by BLO (Fig. 5c). Heatwaves that are associated by AR (Fig. 5b) and AL (Fig. 5d) weather regimes have a frequency of 16% and 24%, respectively. The multidecadal variability in terms of frequency of weather regimes associated to warmest summers is also evident in the study of summer heatwave events. The summer average temperatures for Western Europe (Figure S5, supplementary material) shows higher temperatures in the early and late time span. Those temperature anomalies are more evident once we apply a high criteria to define heatwaves.There is a decrease in the

occurrence of heatwave events during the first half of the 20th century being 1930-1950 the only period with some heatwave events that are more frequently associated with BLO regime. Although the late 19th century is dominated by BLO regime, each weather regime might induce a heatwave event. However, during the late 20th century and the beginning of 21st century, the NAO− regime is scarcely present during heatwave events, which are dominated by AL and, mainly, BLO. We also find that the longest events are associated to BLO regime (Fig. 5c,e).

To shed more light on the circulation changes, we compute composites of SLP and surface temperature anomalies (Fig. 6) during all the days of heatwave events detected in figure 5 divided by periods (table 1). Consistently with Figure 5, most of the heatwave events are concentrated in periods G1 (Fig. 6a) and G4 6d) being NAO- and BLO the mean pressure patterns, respectively, during those periods. There is a change also in the temperature patterns mainly in Northern and Eastern Europe but also in the East coast of North America and the Atlantic Ocean. Similar to G1, G2 (Fig. 6b) has a NAO- as the mean pressure pattern of the period of heatwave events. Although it is the period with scarce occurrence of heatwave events, G3 (Fig. 6c) is dominated by a strong low pressure over the Atlantic ocean (with some influence of BLO over Europe) leading to an increase in temperature anomalies in both East coast of North America and West coast of Europe. Same exercise is repeated but taking into account the occurrence of heatwave events pre-1930 (P1, Fig.6e) and post-1930 (P2, Fig.6f). The temperature pattern changes in pre and post 1930 maps mainly in Greenland and the

East coast of North America and Europe (North and East). Pressure patterns for all the heatwave events pre and post-1930 reproduce well NAO− and BLO-AL (respectively) albeit weaker for the BLO regime which has a strong influence of AL regime (Figure S8, supplementary material). So, even if there is a change for NAO−, BLO is the one with a stronger change for short-term events, because it is the most representative pattern in heatwave events from 1930.

4. Conclusions:

These results confirm that most heat events (either warmest summers and heatwaves in Western Europe) of the second half of the 20th century occurred when the Scandinavian Blocking weather regime dominated the North Atlantic region, causing increasing temperatures and more frequent and longer heatwaves events (figure 5 and figure S9). Our results also show that NAO− is more favorable to drive warm summers before 1930. This early period corresponds to the most frequent co-occurrence of this regime and heatwave events. Although the increasing temperature trends observed during blocking heatwave episodes could be attributed to secular climate change (Coumou et al. 2014), the change in the dominating weather regimes may also be linked to the decadal variability of the atmospheric dynamics. Those findings are consistent with the results of Horton et al. (2015), although we consider heatwaves on a finer spatial scale (Western-Europe). The analysis of Hoffmann (2017) is also complementary to ours, albeit on another region (Postdam, Germany), whose temperature does not respond to

the same atmospheric patterns. However, he found (Figure 11) an increment of two new dominant wave-like patterns with more meridional oscillation, as we have seen for Western Europe at seasonal (Fig. 1, Fig. S2 and Fig. S4) and subseasonal scales (Fig. 5).

The robustness of our results is demonstrated by the use of 20CRv2c 56 ensemble members and other reanalysis datasets (see supplementary material) where we have found similar results. The dynamical analysis also suggests that there is an increase of negative correlations between warmest summers and the NAO− regime.

Although the information extracted in warmest summers and heatwaves is a priori different, our analysis shows similar results at different timescales. In terms of warmest summers, and although there are some evidence of a multidecadal variability of the atmospheric dynamic, NAO− was the most representative pattern up to 1930 and from 1930 on BLO is the most representative one. For short time heat events, the most representative is BLO during the whole period but, as for warmest summers, NAO− events are less frequent after 1930. BLO is associated to the longest and hottest heatwaves and yields an increasing trend, as outlined by Horton et al. (2015).

Acknowledgments:

M.C.A-C. was supported by the Swedish Research Council grant No. C0629701 (MILEX). D.F. was supported by the ERC grant No. 338965–A2C2. P.Y. was supported by the European Unions Seventh Framework Programme grant No.

607085–EUCLEIA. The authors thank G. Compo, for the help supported with data from members of 20CR reanalysis. 20CR and NCEP Reanalysis data were provided by the NOAA/OAR/ESRL PSD, Boulder, Colorado, USA, and retrieved from https://climatedataguide.ucar.edu/climate-data/noaa-20th-century-reanalysis-version-2-and-2c and http://www.esrl.noaa.gov/psd/. ERA-20C reanalysis data provided by the ECMWF (European Centre for Medium-Range Weather Forecasts), Reading, UK, from their website at http://apps.ecmwf.int/datasets/data/era20c-daily/. The authors declare that there is no conflict of interest regarding the publication of this paper.

Supplementary Material:

- Figure S1: Boxplots of Absolute Root Mean Square Error by period and weather regime.
- Figure S2: Relative long-term summer weather regime frequency over the North-Atlantic region and their dominance in warmest summers in Western-Europe (1871-2015) using three reanalysis products (20CR, ERA20C, NCEP).
- Figure S3: Temperature anomalies during warmest summers in Western Europe with dominance of each weather regime in three reanalysis products (20CR, ERA20C, NCEP).
- Figure S4: 31-years running correlation of the Weather Regimes frequency and the mean temperature in western Europe (20CRv2c)
- Figure S5: Summer average temperatures for Western Europe for three reanalysis

products (20CR, ERA20C, NCEP).

- Figure S6: Dynamical representation of the warmest summers for ERA20C during 1900-2010 in regimes AR-NAO- and BLO-AL.
- Figure S7: Dominants weather regimes during Summer Heatwave events in Western-Europe for three reanalysis products (20CR, ERA20C, NCEP).
- Figure S8: SLP anomalies in heatwave events (20CRv2c EM) for each period,
- Figure S9: Temperature (y-axis) vs numbers of days (x-axis) during each heatwave event for the 20CR Ensemble Mean (1871-2011) weather regimes.
- Table S1: Absolute root mean square error by period and weather regime.

Correspondence and requests for further materials should be addressed to M.C.A-C (email: carmen.alvarez-castro@lsce.ipsl.fr).

References:

Casdagli, M., Eubank, S., Farmer, J. D. & Gibson, J. (1991). State space reconstruction in the presence of noise, *Physica D.* **51**(1): 52–98.

Cassou, C., Terray, L. & Phillips, A. S. (2005). Tropical atlantic influence on European heat waves, *J. Climate* **18**(15): 2805–2811.

Chekroun, M. D., Simonnet, E. & Ghil, M. (2011). Stochastic climate dynamics: Random attractors and time-dependent invariant measures, *Physica D.* **240**(21): 1685–1700.

Ciais, P. et al. (2005). Europe-wide reduction in primary productivity caused by the heat and drought in 2003, *Nature* **437**(7058): 529–533.

Compo, G. P. et al. (2011). The twentieth century reanalysis project, *Q. J. Roy. Meteor. Soc.* **137**(654): 1–28.

328 Corti, S., Molteni, F. & Palmer, T. (1999). Signature of recent climate change in frequencies of natural
329 atmospheric circulation regimes, *Nature* **398**(6730): 799–802.

330 Coumou, D., Petoukhov, V., Rahmstorf, S., Petri, S. & Schellnhuber, H. J. (2014). Quasi-resonant
331 circulation regimes and hemispheric synchronization of extreme weather in boreal summer,
332 *Proceedings of the National Academy of Sciences* **111**(34): 12331–12336.

333 Della-Marta, P. M., Luterbacher, J., von Weissenfluh, H., Xoplaki, E., Brunet, M. & Wanner, H. (2007).
334 Summer heat waves over western Europe 1880–2003, their relationship to large-scale forcings
335 and predictability, *Clim. Dynam.* **29**(2-3): 251–275.

336 Fischer, E., Seneviratne, S., Lüthi, D. & Schär, C. (2007). Contribution of land-atmosphere coupling
337 to recent European summer heat waves, *Geophys. Res. Lett.* **34**(6).

338 Hoffmann, P. (2017). Enhanced seasonal predictability of the summer mean temperature in Central
339 Europe favored by new dominant weather patterns, *Climate Dynamics.* .
340 **URL:** *https://doi.org/10.1007/s00382-017-3772-0*

341 Horton, D. E., Johnson, N. C., Singh, D., Swain, D. L., Rajaratnam, B. & Diffenbaugh, N. S. (2015).
342 Contribution of changes in atmospheric circulation patterns to extreme temperature trends,
343 *Nature* **522**(7557): 465–469.

344 Jézéquel, A., Yiou, P. & Radanovics, S. (2017). Role of circulation in european heatwaves using flow
345 analogues, *Climate Dynamics* .
346 **URL:** *https://doi.org/10.1007/s00382-017-3667-0*

347 Kalnay, E. et al. (1996). The NCEP/NCAR 40-year reanalysis project, *B. AM. Meteorol. Soc.*
348 **77**(3): 437–471.

349 Katok, A. & Hasselblatt, B. (1997). *Introduction to the modern theory of dynamical systems*, Vol. 54,
350 Cambridge University Press.

351 Lorenz, E. N. (1991). Dimension of weather and climate attractors, *Nature* **353**(6341): 241–244.

352 Meehl, G. A. & Tebaldi, C. (2004). More intense, more frequent, and longer lasting heat waves in the
353 21st century, *Science* **305**(5686): 994–997.

354 Michelangeli, P.-A., Vautard, R. & Legras, B. (1995). Weather regimes: Recurrence and quasi
355 stationarity, *J. Atmos. Sci.* **52**(8): 1237–1256.

356 Mueller, B. & Seneviratne, S. I. (2012). Hot days induced by precipitation deficits at the global scale,
357 *Proc. Natl. Acad. Sci.* **109**(31): 12398–12403.

358 Poli, P. et al. (2013). The data assimilation system and initial performance evaluation of the ecmwf
359 pilot reanalysis of the 20th-century assimilating surface observations only (ERA-20C), *ECMWF*
360 *ERA Rep* **14**: 59.

361 Poumadere, M., Mays, C., Le Mer, S. & Blong, R. (2005). The 2003 heat wave in France: dangerous
362 climate change here and now, *Risk Anal.* **25**(6): 1483–1494.

363 Quesada, B., Vautard, R., Yiou, P., Hirschi, M. & Seneviratne, S. I. (2012). Asymmetric European
364 summer heat predictability from wet and dry southern winters and springs, *Nature Clim. Change*
365 **2**(10): 736–741.

366 Robine, J.-M., Cheung, S. L. K., Le Roy, S., Van Oyen, H., Griffiths, C., Michel, J.-P. & Herrmann,
367 F. R. (2008). Death toll exceeded 70,000 in Europe during the summer of 2003, *C. R. Biol.*
368 **331**(2): 171–178.

369 Schär, C. & Jendritzky, G. (2004). Climate change: hot news from summer 2003, *Nature*
370 **432**(7017): 559–560.

371 Schär, C., Lüthi, D., Beyerle, U. & Heise, E. (1999). The soil-precipitation feedback: A process study
372 with a regional climate model, *J. Climate* **12**(3): 722–741.

373 Stefanon, M., D'Andrea, F. & Drobinski, P. (2012). Heatwave classification over Europe and the
374 Mediterranean region, *Environ. Res. Lett.* **7**(1): 014023.

375 Stott, P. A., Stone, D. A. & Allen, M. R. (2004). Human contribution to the European heatwave of
376 2003, *Nature* **432**(7017): 610–614.

377 Vautard, R., Yiou, P., D'andrea, F., De Noblet, N., Viovy, N., Cassou, C., Polcher, J., Ciais, P.,
378 Kageyama, M. & Fan, Y. (2007). Summertime European heat and drought waves induced by
379 wintertime Mediterranean rainfall deficit, *Geophys. Res. Lett.* **34**(7).

Wreford, A. & Adger, W. N. (2010). Adaptation in agriculture: historic effects of heat waves and droughts on UK agriculture, *Int. J. Agric. Sustain.* **8**(4): 278–289.

Yiou, P. et al. (2008). Weather regime dependence of extreme value statistics for summer temperature and precipitation, *Nonlinear Proc. Geoph.* **15**(3): 365–378.

Zampieri, M., D'Andrea, F., Vautard, R., Ciais, P., de Noblet-Ducoudré, N. & Yiou, P. (2009). Hot European summers and the role of soil moisture in the propagation of mediterranean drought, *J. Climate* **22**(18): 4747–4758.

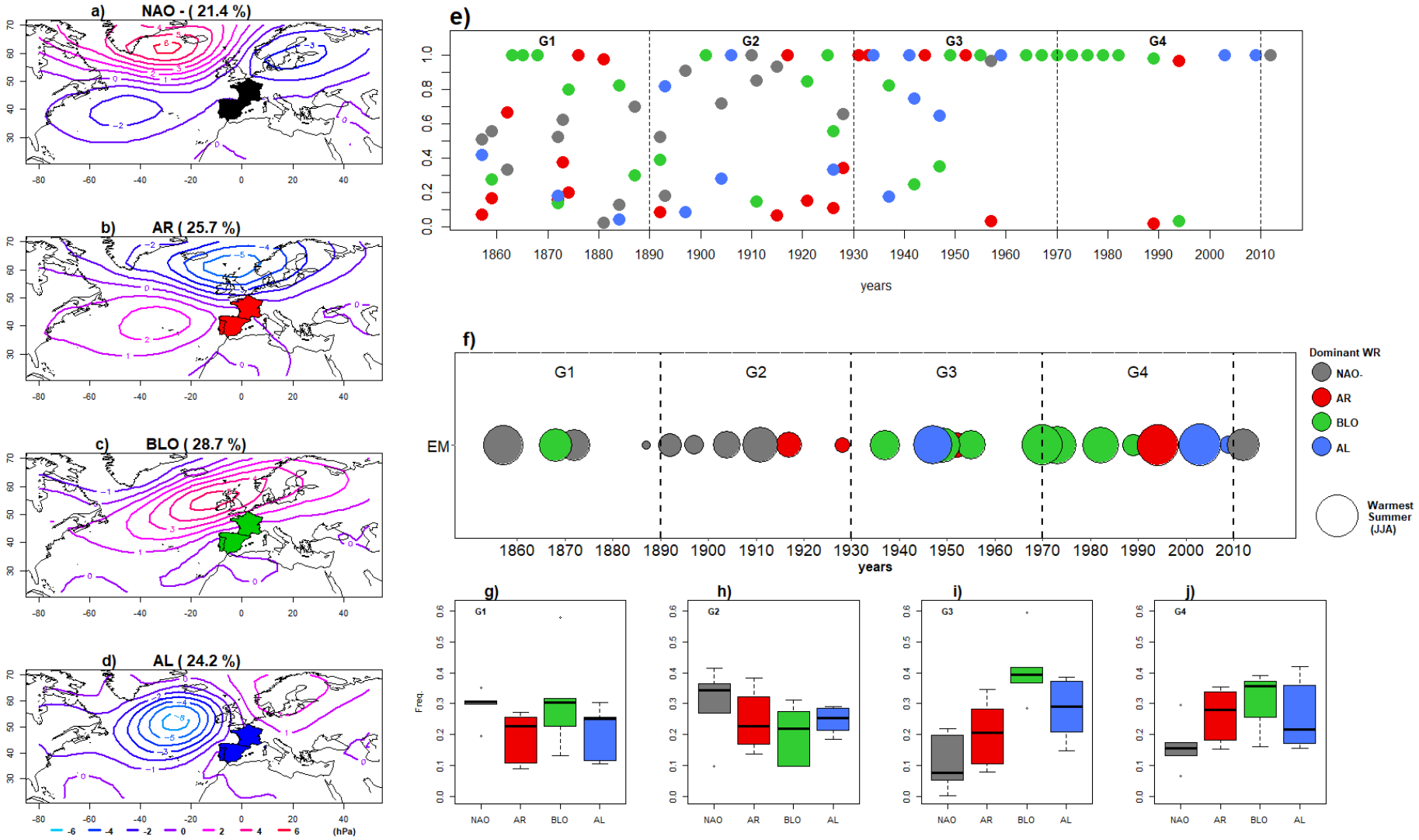

Figure 1. Summer SLP weather regimes over the North-Atlantic region and their dominance in the twenty warmest summers during 1871-2011 in Western-Europe. a-d, Summer SLP (hPa anomalies) Weather regimes: **a,** North Atlantic Oscillation in its negative phase (NAO−). **b,** Atlantic Ridge (AR). **c,** Blocking (BLO). **d,** Atlantic Low (AL) weather regime. **e,**Probability to find a dominant weather regime in all the warmest summers (EM and 56 members).**f,** 24 warmest summers in Western-Europe (colored region in **a-d**) with their dominant weather regime (20CRv2c EM). Circle size depends on temperature (anomalies), the largest the warmest. Colors represents the dominant weather regime for each summer based in the highest anomalous frequency. **g-j,** Boxplots of daily weather regimes during the 24 warmest summers of 20CRv2c EM (as in **f**) in Western-Europe separated by groups of 6 summers per 40 years: **g,** shows group G1, **h,** group G2, **i** group G3, and **j**group G4 1.

Table 1. Groups and periods used during the analysis of 20CRv2c (EM and 56 members of the ensemble).

Group	Years	Period
G1	1851-1890	
		P1
G2	1891-1930	
G3	1931-1970	
		P2
G4	1971-2010	

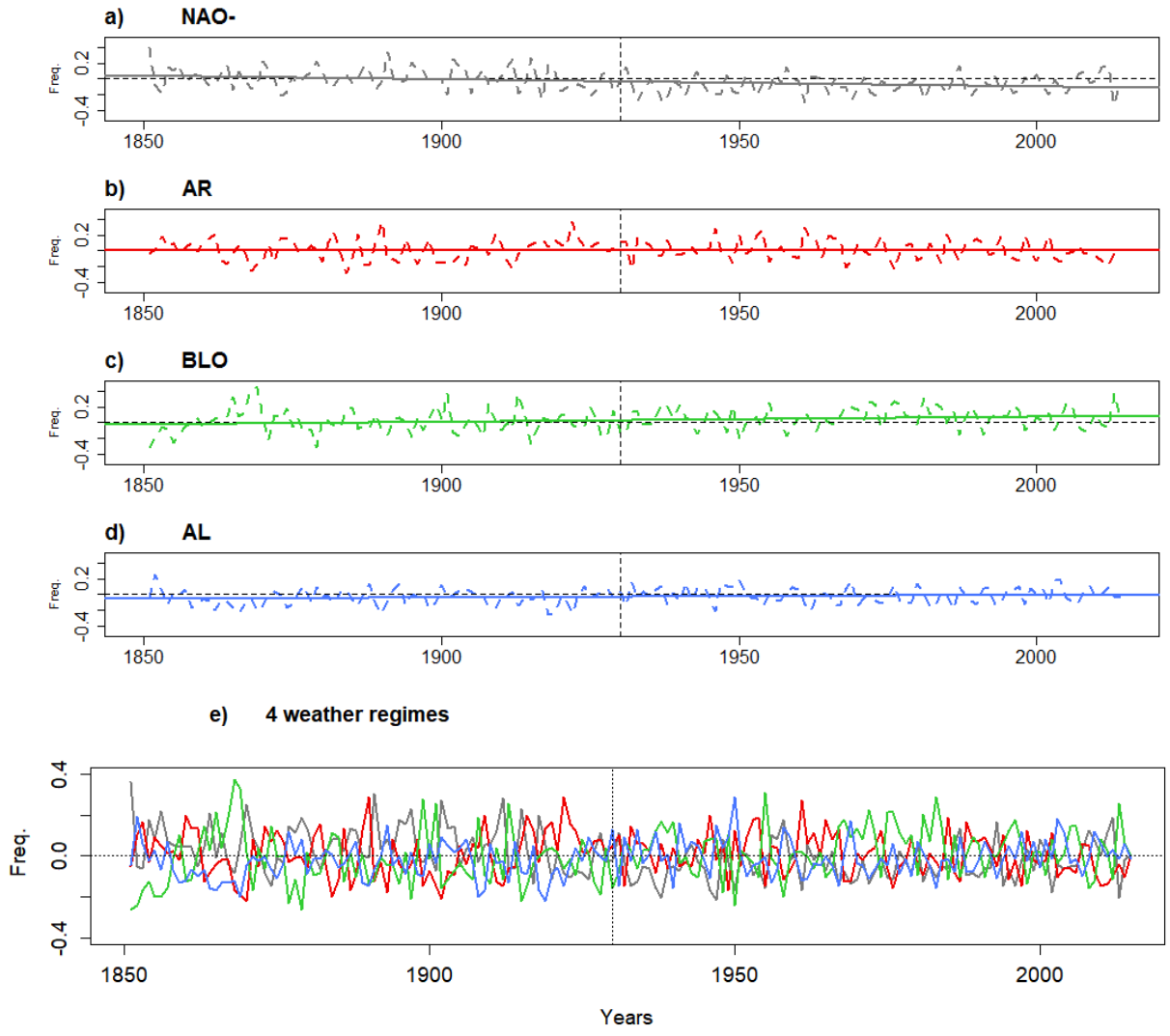

Figure 2. Relative long-term summer weather regime frequency. Relative frequency of summer SLP (hPa) weather regimes over the North-Atlantic region (1851-2014) using 20CRv2c. Here we show SLP anomalies with respect to the reference period 1970-2010 for each (a-d) and all (e) weather regimes , solid lines in a-d) represents the linear trend for each regime. 1930 it is marked with a vertical dashed line.

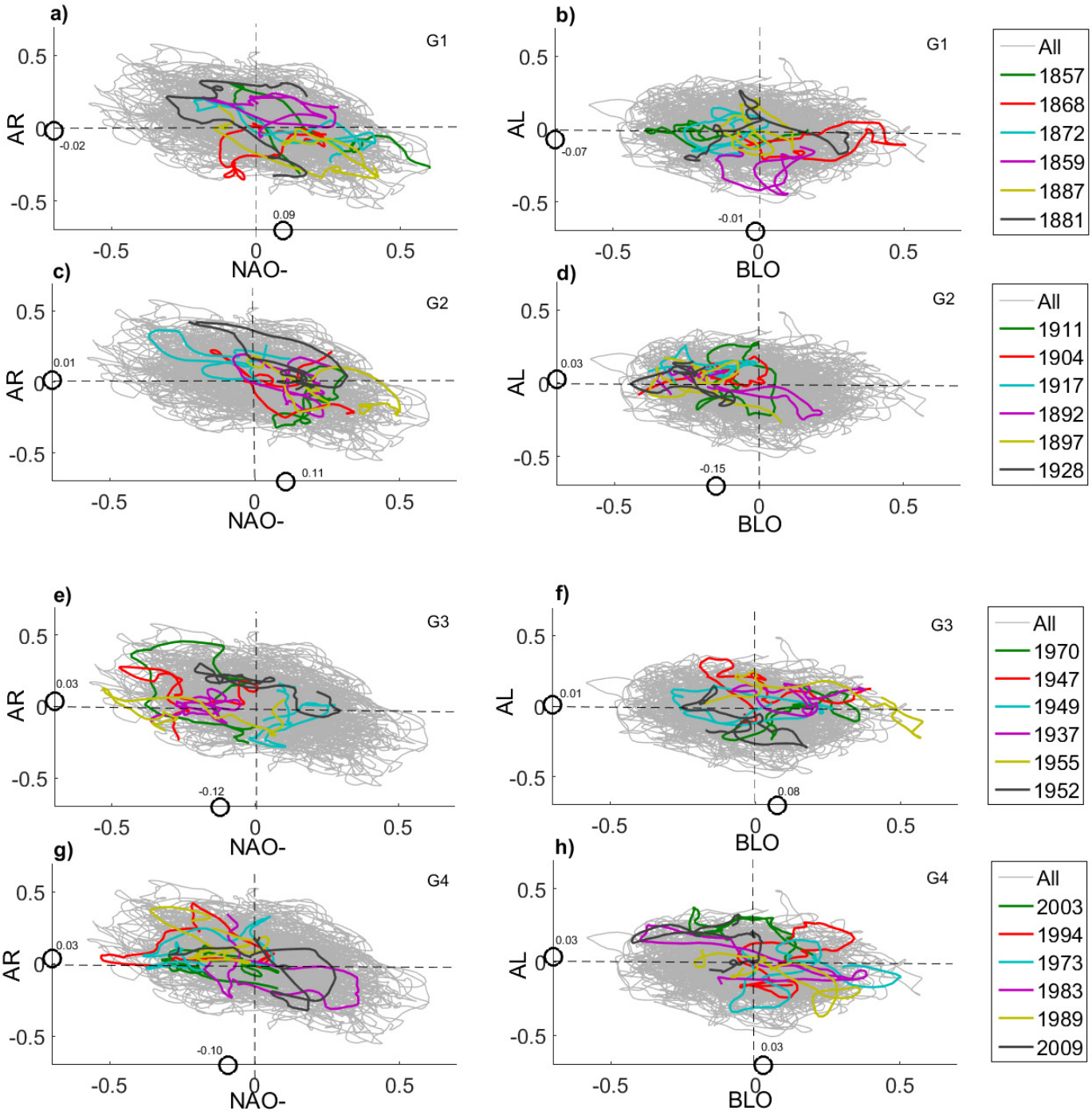

Figure 3. Dynamical representation of the warmest summers. Correlations of daily SLP fields and NAO− (x-axis), AR (y-axis) (top) and AL , BLO (bottom) weather regimes for the 4 groups of summers. Warmest summers are colored as in the legend with, light grey lines represent all data. Average correlations of warmest summers with respect to the NAO− weather regimes (black circle on x-axis). A moving average filter of 30 days window was applied to the warmest summers for better representation.

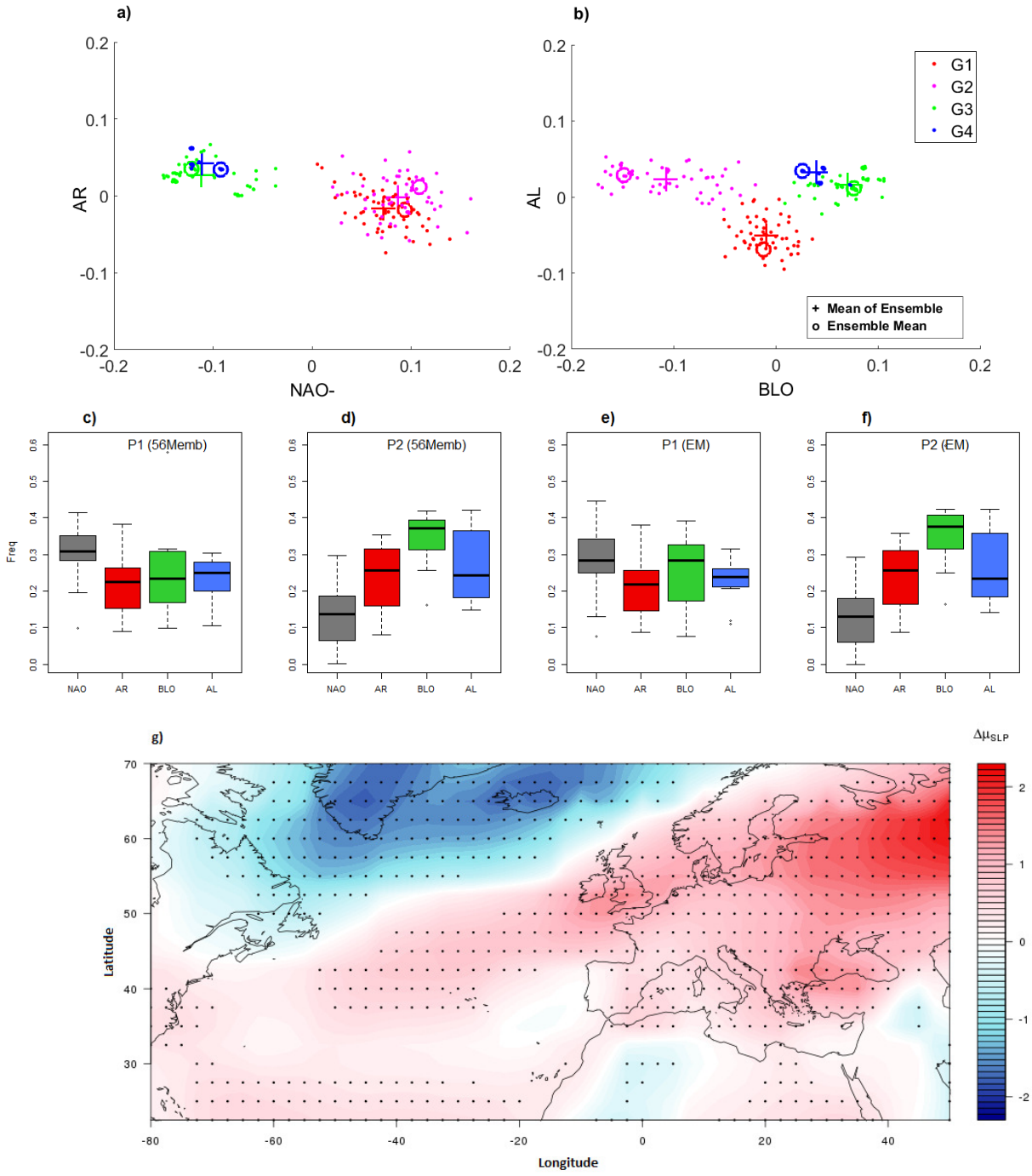

Figure 4. Changes in the dynamical representation of the warmest summers. **a-b,** Average correlations of warmest summers with respect to the 4 weather regimes (black circle on x-axis in Figure 3), points represents each member, crosses represents the mean of all the 56 members and circles represent the EM. Colors represents the 4 groups of summers (G1 red, G2 purple, G3 green, G4 blue). In **c-f** boxplots showing frequencies of the 4 weather regimes classified in two periods: **c,e** for summers before 1930 (groups G1+G2) and **d,f** for summers after 1930 (groups G3+G4), for all the 56 members **(c-d)** and the EM **(e-f)**. **g,** shows the difference in the SLP mean between those two periods (after1930- before 1930). Points represents significativity at 95 percent after the performance of a Montecarlo test.

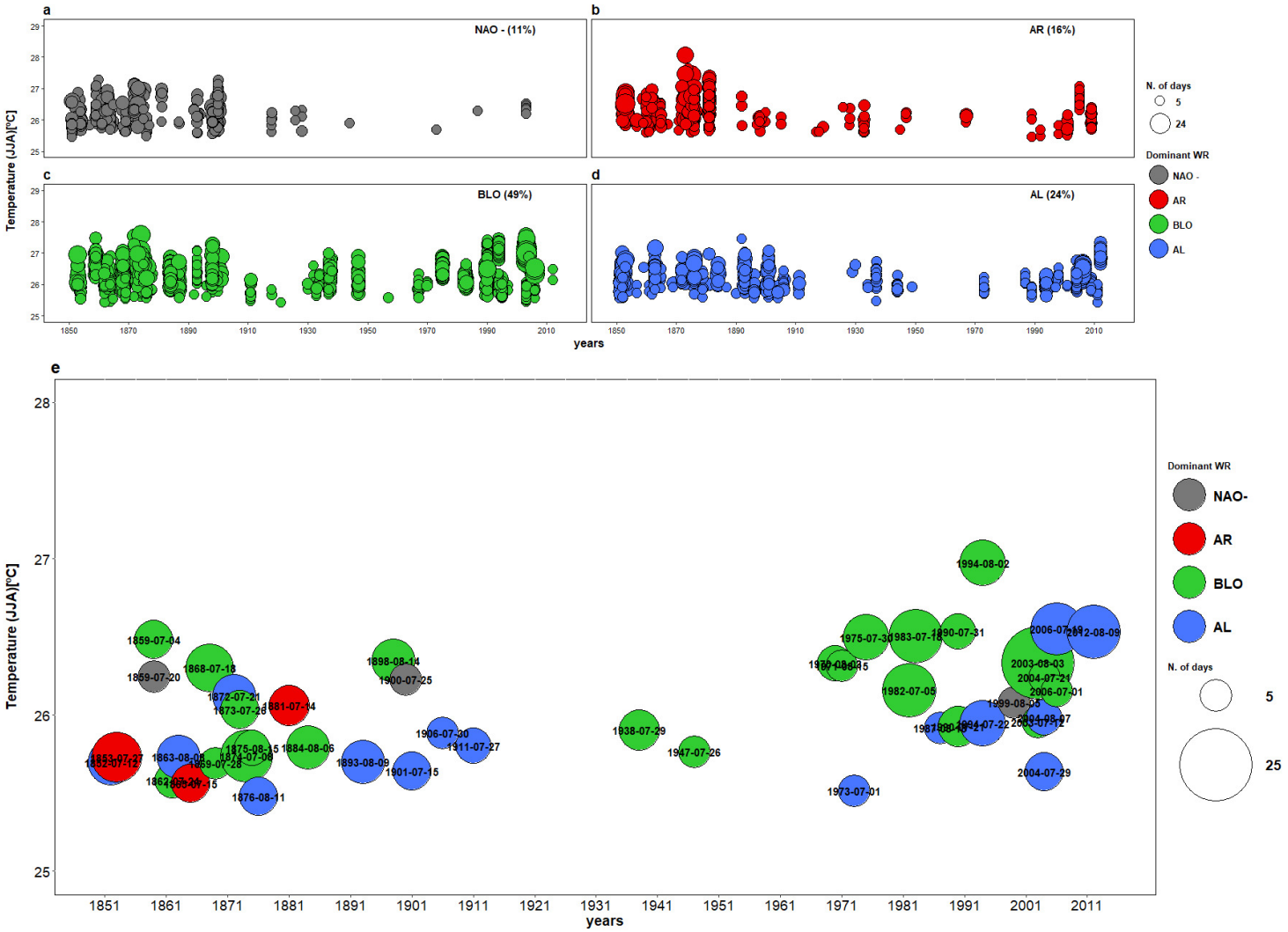

Figure 5. Dominant weather regimes during Summer heatwave events. In **a–d,** Summer heatwave events (95th Percentile) for all the members and **e,** EM (circles with stars) of 20CR data, 1851–2014. Colors correspond to the dominant weather regime in each event, temperature (y-axis) and years (x-axis). Circle sizes depend on the event duration by number of days, the larger the longer duration.

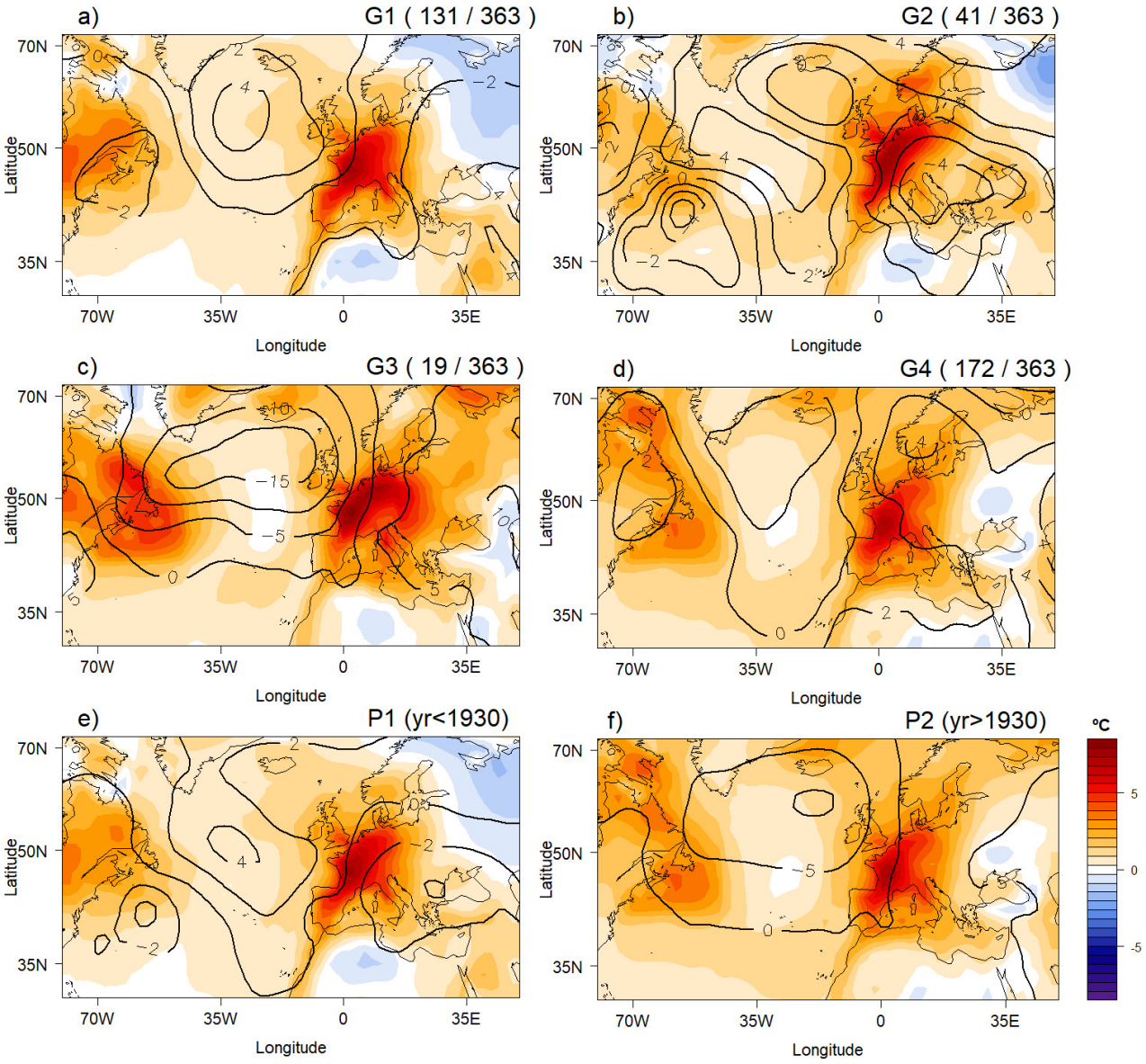

Figure 6. Composites of Sea Level Pressure (SLP) and Surface Temperature anomalies (SAT) during heatwaves events. In **a–d,** composites SLP (hPa) and SAT (°C) anomalies for all the days during heatwaves events in each period, from G1 to G4, in **e,** anomalies for all the days during heatwaves events before 1930 and **f,** after 1930.

Atmospheric dynamics leading to West European summer hot temperatures since 1851

M. Carmen Alvarez-Castro, Davide Faranda, Pascal Yiou

Laboratoire des Sciences du Climat et de l' Environnement, UMR 8212
CEA-CNRS-UVSQ, IPSL, Université Paris-Saclay, F-91191 Gif-sur-Yvette, France

E-mail: carmen.alvarez-castro@lsce.ipsl.fr

November 2017

Supplementary Material

- Figure S1: Boxplots of Absolute Root Mean Square Error by period and weather regime.
- Figure S2: Relative long-term summer weather regime frequency over the North-Atlantic region and their dominance in warmest summers in Western-Europe (1871-2015) using three reanalysis products (20CR, ERA20C, NCEP).
- Figure S3: Temperature anomalies during warmest summers (IP-France) with dominance of each weather regime in three reanalysis products (20CR, ERA20C, NCEP).
- Figure S4: 31-years running correlation of the Weather Regimes frequency and the mean temperature in western Europe (20CRv2c)
- Figure S5: Summer average temperatures for Western-Europe for three reanalysis products (20CR, ERA20C, NCEP).
- Figure S6: Dynamical representation of the warmest summers for ERA20C during 1900-2010 in regimes AR-NAO- and BLO-AL.
- Figure S7: Dominants weather regimes during Summer Heatwave events in Western-Europe for three reanalysis products (20CR, ERA20C, NCEP).
- Figure S8: SLP anomalies in heatwave events (20CRv2c EM) for each period,
- Figure S9: Temperature (y-axis) vs numbers of days (x-axis) during each heatwave event for the 20CR Ensemble Mean (1871-2011) weather regimes.
- Table S1: Absolute root mean square error by period and weather regime.

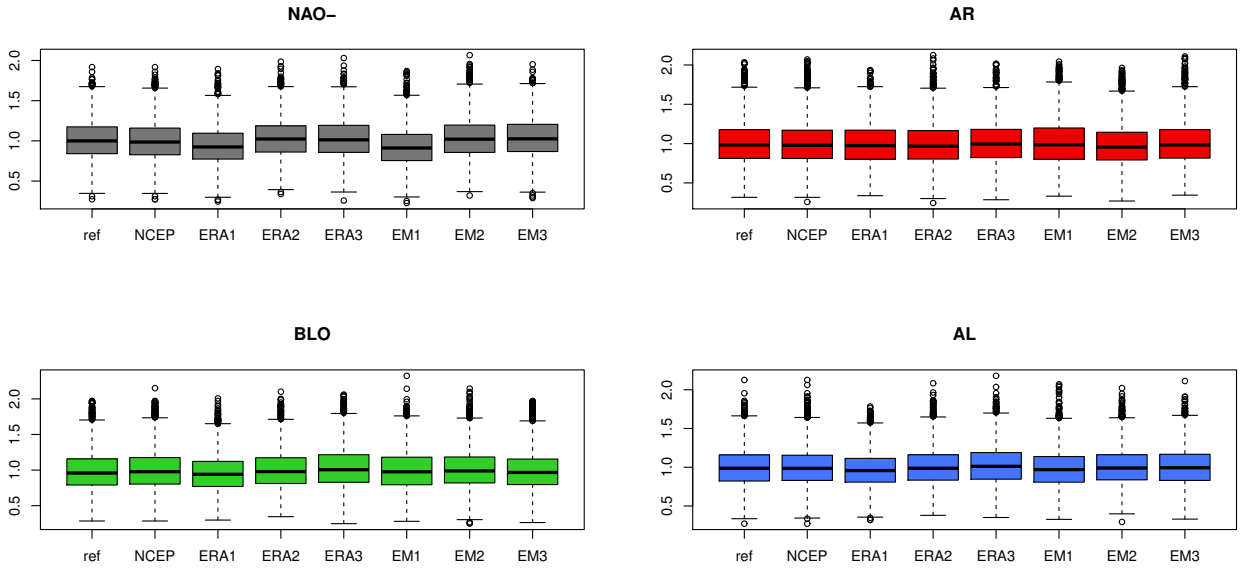

Figure S 1. Boxplots of Absolute Root Mean Square Error by period and weather regime. Colors represent each weather regime. (See also Table S1).

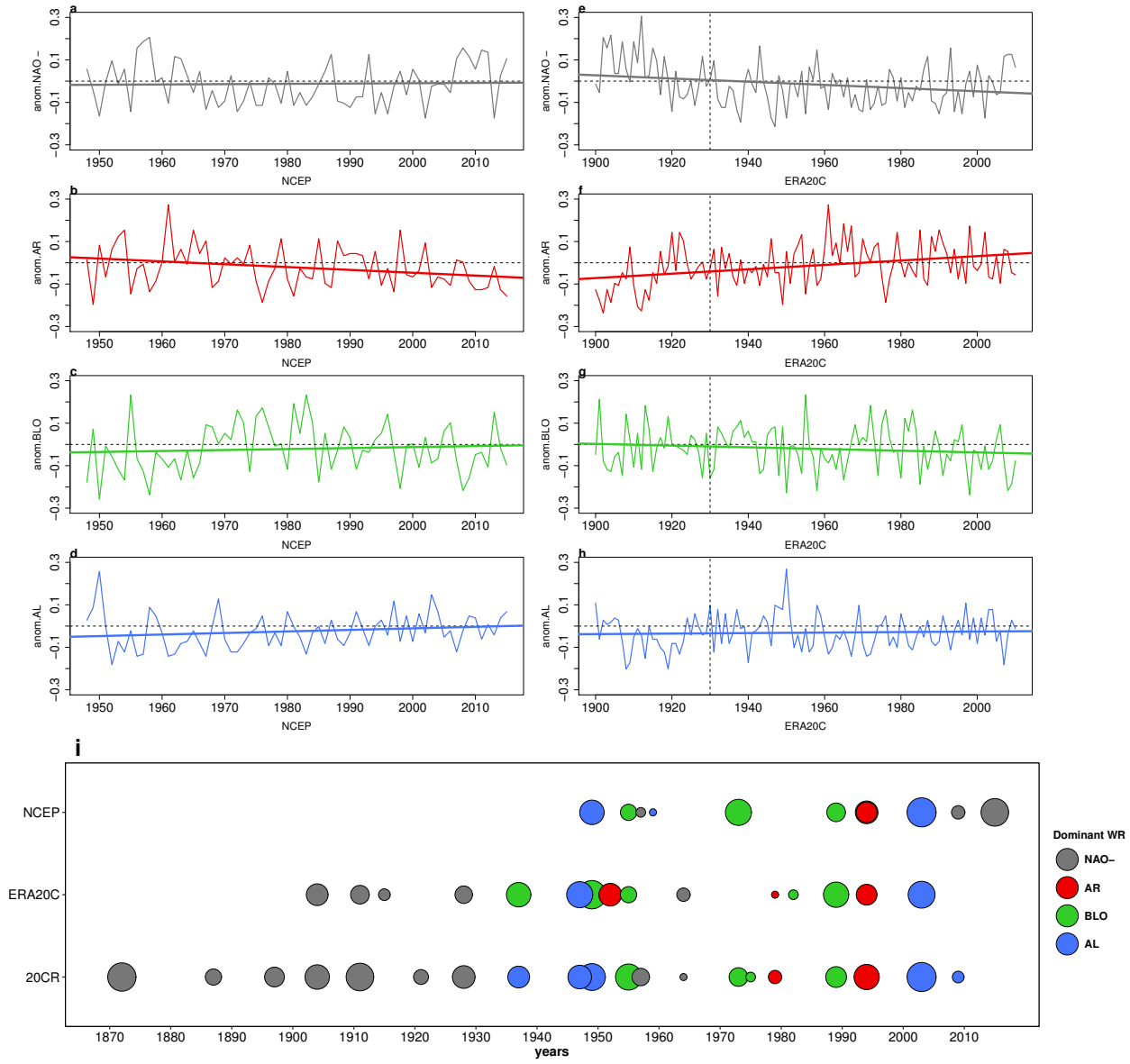

Figure S 2. Relative long-term summer weather regime frequency over the North-Atlantic region and their dominance in warmest summers in Western-Europe (1871-2016) using three reanalysis products (20CR, ERA20C, NCEP). As in figure S1, relative frequency of Summer SLP (hPa anomalies) weather regimes: NAO- (**a,e**), AR (**b,f**), BLO (**c,g**) and AL (**d,h**), but considering NCEP data (**a-d,**) and ERA20C (**e-h**). **e,** Warmest summers from 1871 to 2015 in Western-Europe with their dominant weather regime. Years are shown in x axis while y axis display each of the reanalysis products (20CR, ERA20C, NCEP). Circle size depends on temperature anomalies, the largest the warmest. Colors (black, red, green, blue) represents the dominant weather regime (NAO-, AR, BLO, AL) for each summer. The number of warmest summers are ponderate with the length of each dataset.

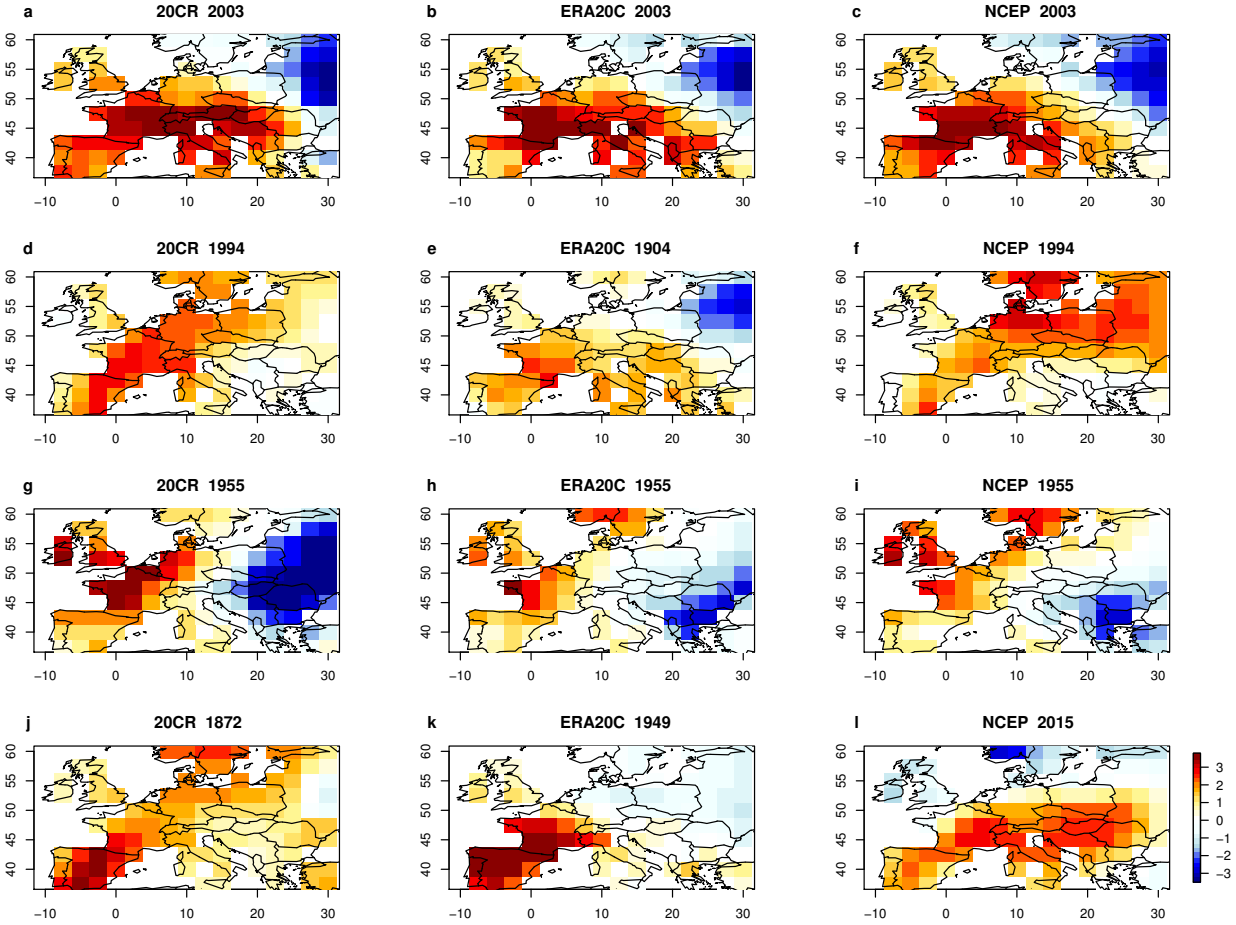

Figure S 3. Temperature anomalies maps for warmest summers in Western-Europe. Each row correspond to a different dominant weather regime for some explanatory summers. Each column is a different reanalysis product.**a-c,** Summer 2003, where AL was the dominant weather regime. **d-f,** Summer of 1994, where AR was the dominant weather regime (Same frequencies of BLO and AR for NCEP during this summer). **g-i,** Summer of 1955, where BLO was the dominant weather regime. **j-l,** Since there is not a common summer for all the reanalysis datasets with NAO- as a dominant weather regime, here we show the most warmest summer (1872, 1904, 2015) where NAO- was the dominant weather regime in each reanalysis dataset (20CR, ERA20C, NCEP).

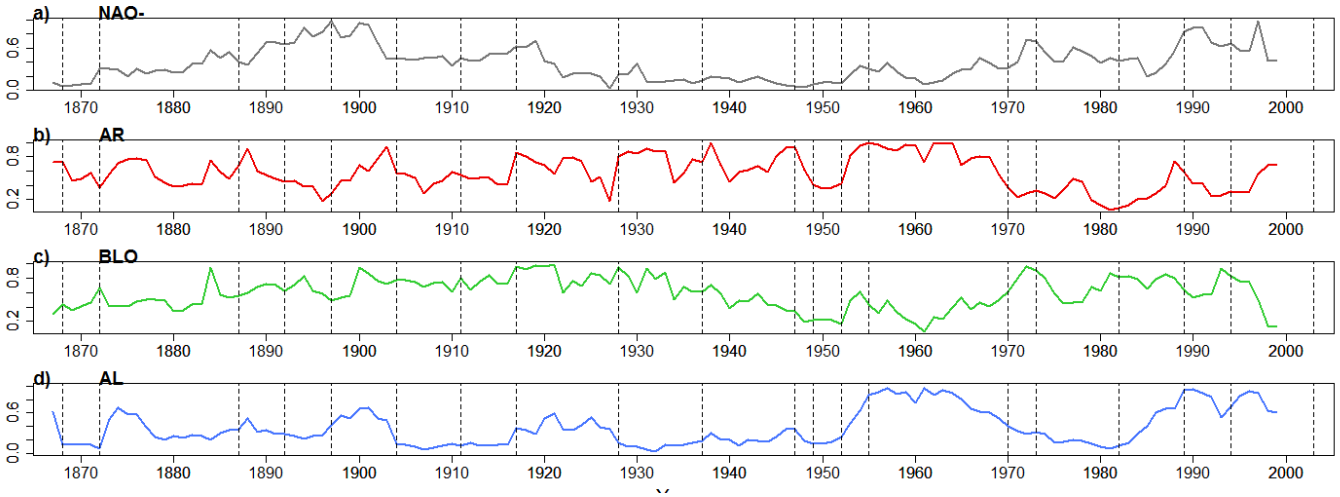

Figure S 4. 30yr-running correlations of summer mean temperatures and weather regime frequency in Western Europe. The data used is the Ensemble Mean of 20CRv2c. Warmest summers are marked with a vertical dashed line.Colors represents the weather regimes

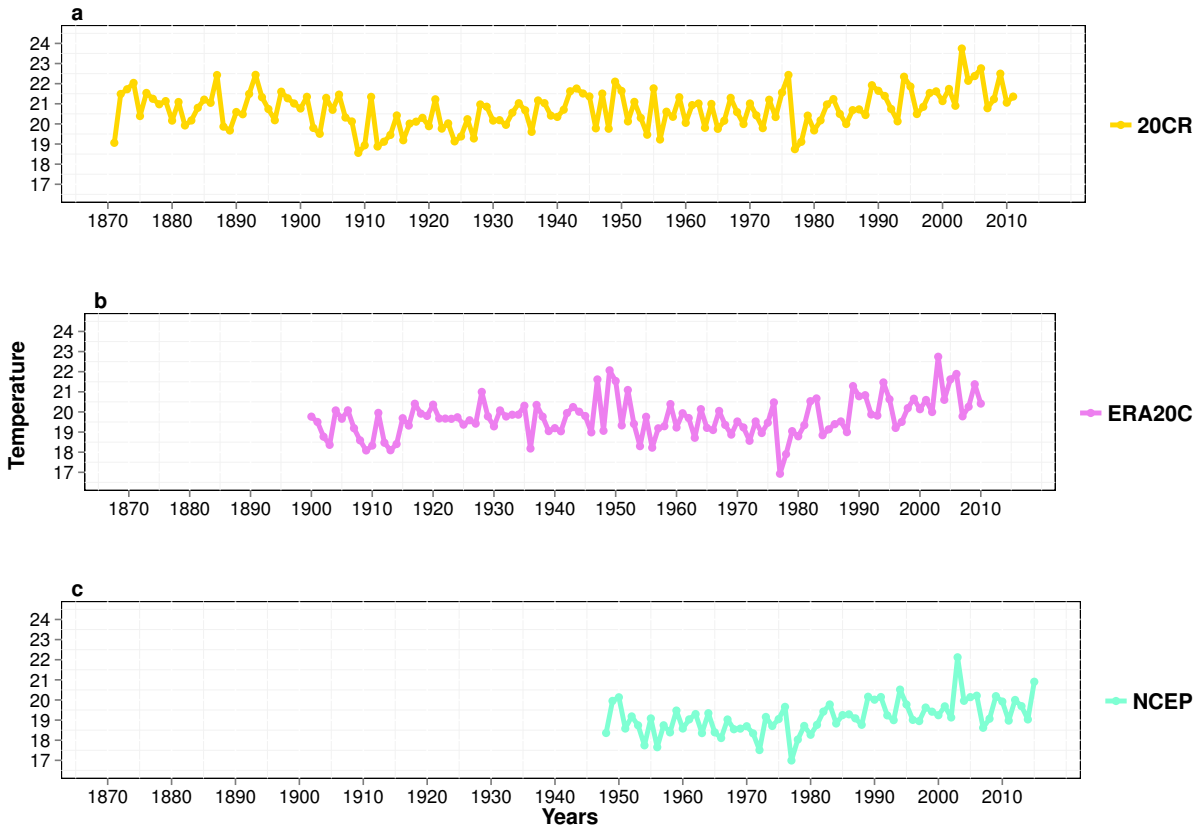

Figure S 5. Summer average temperatures (°C) for Western-Europe. a, 20CR **b,** ERA20C and **c,** NCEP).

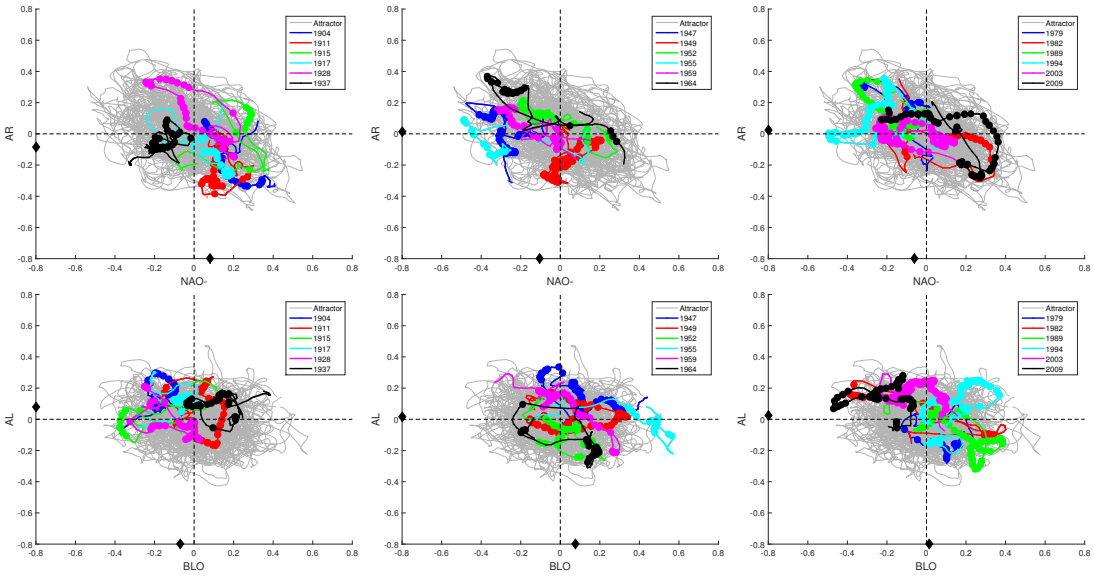

Figure S 6. Dynamical representation of the warmest summers (same as fig.3 in main text) for ERA20C during 1900-2010. Correlations of daily SLP fields and NAO- (x-axis), AR (y-axis) weather regimes in upper panels and correlations of daily SLP fields and BLO (x-axis), AL (y-axis) weather regimes in the bottom panels for three different periods. Warmest summers are colored as in the legend, light grey lines represent all data. Big circles represent days with temperature above 85th percentile. Average correlations of warmest summers with respect to each weather regime (black circle on x-axis). A moving average filter of 30 days window was applied to the warmest summers for better representation.

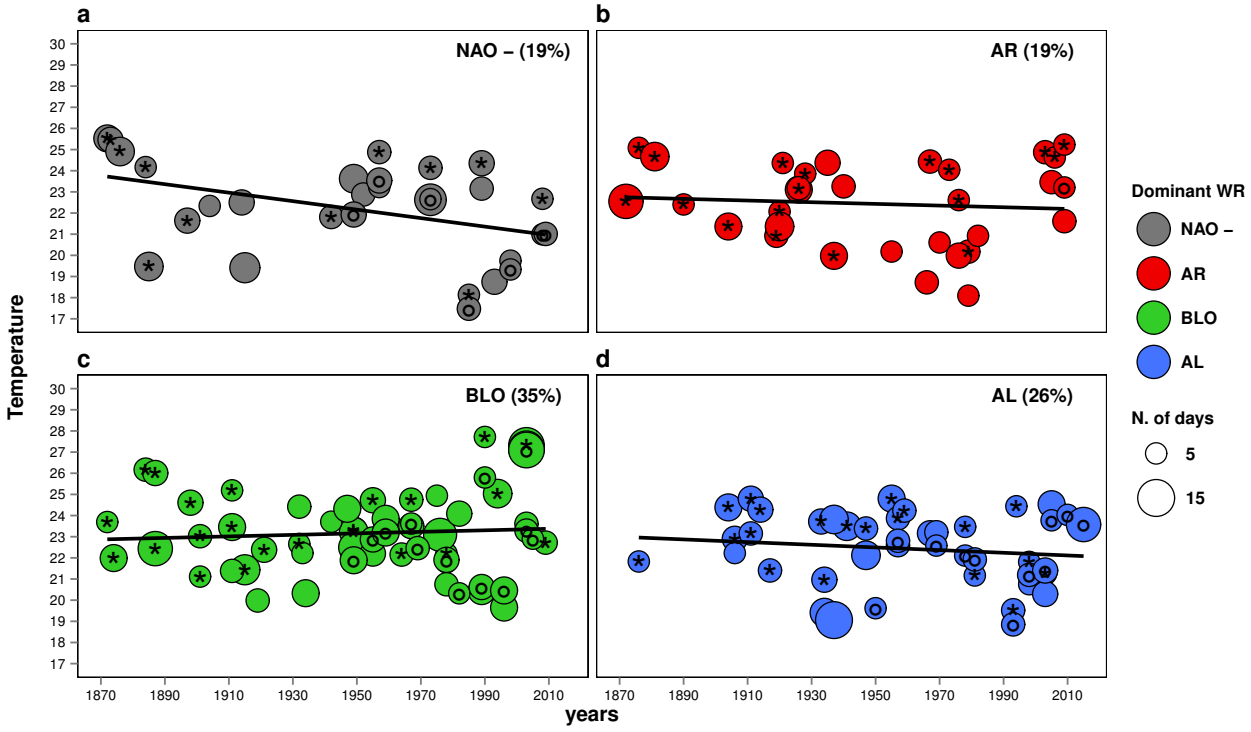

Figure S 7. Dominant weather regimes during Summer Heatwave events in Western-Europe. Summer heatwave events (P90th Percentile) from 1871 to 2015 for different reanalysis products: 20CR (circle with stars), ERA20C (empty circle), and NCEP (circles with inner circle). Colors correspond to the dominant Weather regime (**a-d,**) in each event, temperature (y-axis) and years (x-axis). Circle sizes depend on the event duration by number of days, the larger the longer duration. Percentages show the frequency of each weather regime. Linear fits are shown in black solid lines.

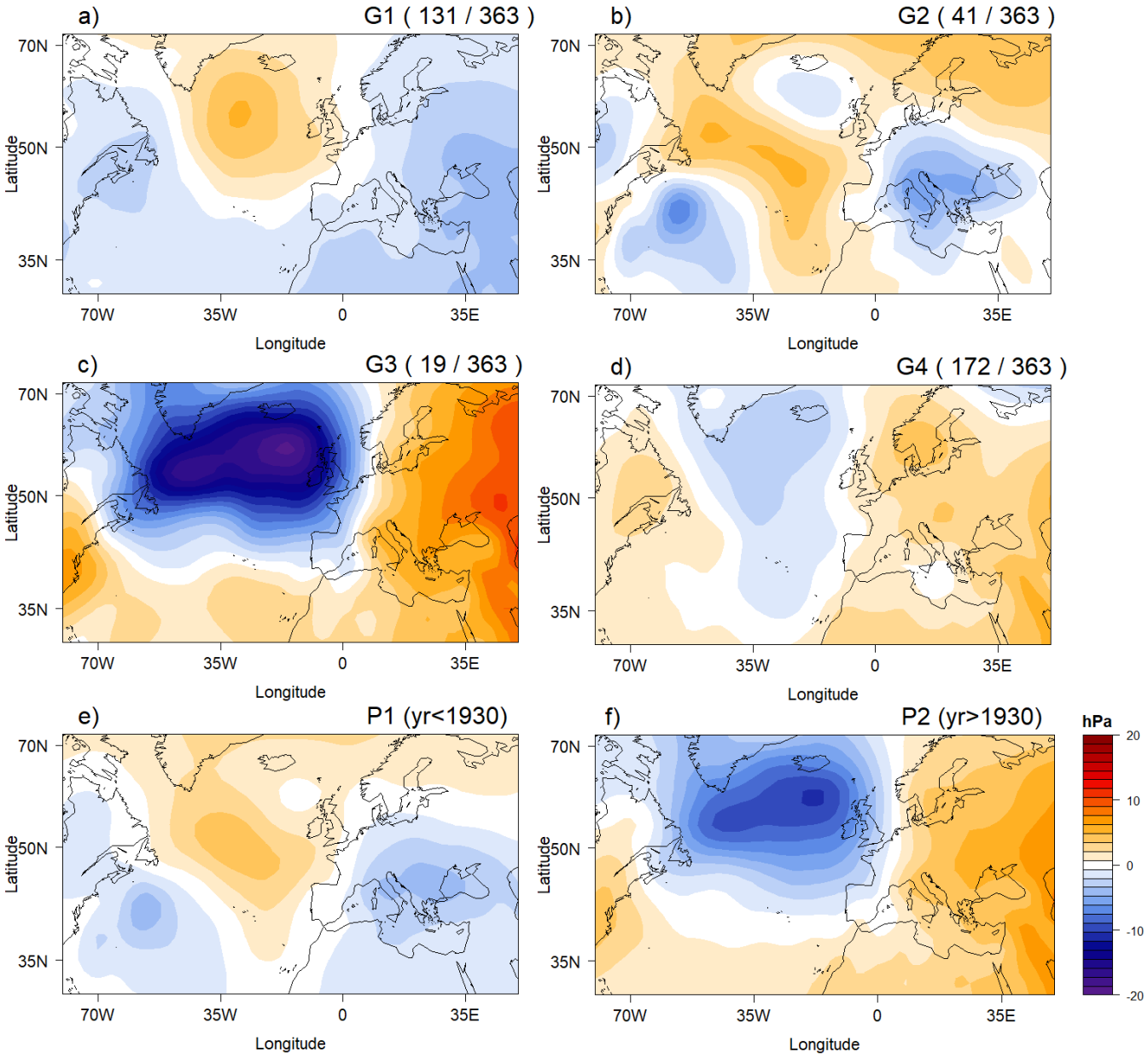

Figure S 8. mean SLP anomalies in heatwave events (20CRv2c EM) for each period. As figure 6, a-d show mean SLP anomalies in heatwaves events for each group of years. Numbers at the top right corner represent the number of heatwave events during that period in comparison with the total number of heatwave events in 20CRv2c EM. Mean SLP anomalies in heatwaves events pre-1930 and post-1930 are represented in e-f, respectively.

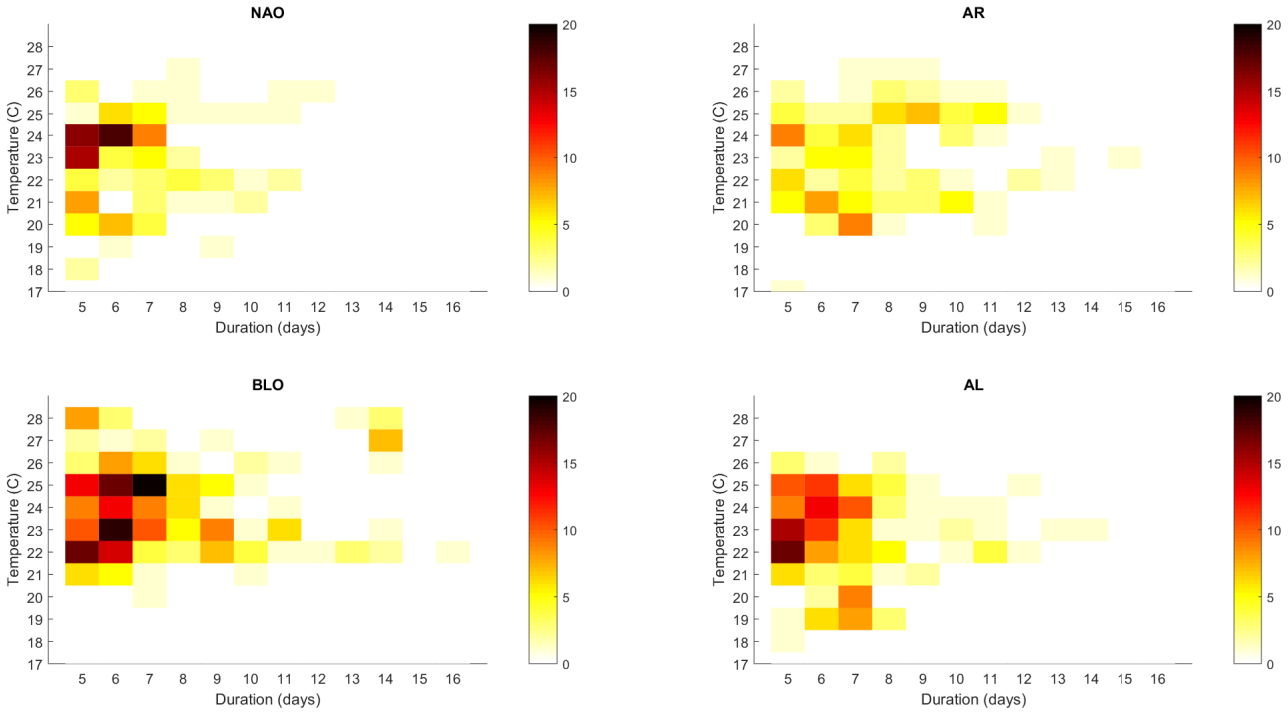

Figure S 9. Density plot of heatwave events. Temperature (y-axis) vs numbers of days (x-axis) during each heatwave event for the 20CR Ensemble Mean (1871-2011) weather regimes. Colors represent the number of hetwaves events.

Abs_{RMSE}	**Period**	**NAO-**	**AR**	**BLO**	**AL**
NCEP	**(1970-2010)**	**1.01**	**1.00**	**0.98**	**0.99**
	(1948-2015)	1.01	1.0	1.01	1.00
ERA 20C	(1900-1936)	0.95	0.99	0.96	0.97
	(1937-1973)	1.03	0.99	1.01	1.01
	(1974-2010)	1.03	1.01	1.03	1.03
20CR	(1871-1917)	0.94	1.01	1.00	0.99
	(1918-1964)	1.03	0.98	1.02	1.01
	(1965-2011)	1.04	1.01	0.99	1.01

Table S 1. Absolute error of the Root mean square deviation (Abs_{RMSE}) of the truncated EOFs during the training period(NCEP:1970-2010) by Weather Regimes during summer in Western-Europe (see also Figure S1)